Zeeman Effect

PHYS3111 - Quantum Mechanics

Toby Nguyen - z5416116

Contents

1 Introduction

On March 12, 1862, Faraday carried out his last experiment in the laboratory of the Royal Institution. Despite his notes not being completely clear, it was obvious he was trying to demonstrate that magnetism has a direct effect on light sources through the use of a spectroscope. He found nothing and even wrote "not the slightest effect demonstrable either with polarised or unpolarised light." This would lead Maxwell to proclaim at a meeting of the British Association on September 15, 1870 that light-radiating particles in a flame could not be altered by any natural force, even in the slightest, either in their mass or perid of oscillation. Nowadays, this would be quite surprising coming from the grandfather of electromagnetic theory.

In August of 1896, Pieter Zeeman placed a sodium flame inbetween the poles of a strong electromagnet, exposing the flame to a large magnetic field. The spectral lines created by observing the flame through a Rowland mirror had broadened once the magnetic field was turned on and were sharply defined in absence of a magnetic field. Initially, Zeeman and his colleagues dismissed the result, as guided by the powerful words by the now late James Clerk Maxwell years prior, no natural force could alter the oscillations of the light particles in a flame.

However, they would soon confirm their results by changing the direction of observation. First, they looked at the spectral lines perpendicular to the magnetic field, seeing the broadening of the spectral lines. Then, they observed the flame parallel to the magnetic field, now seeing a strange splitting of the same lines. Later formalised into a paper with the help of fellow electromagnetic savant, Hendrik Lorentz, the pair would describe three-colour light coming from the source when viewed perpendicular to the magnetic field and two-colour light coming from the source when viewed parallel to the magnetic field in place of the one-colour light when there is no magnetic field.

The Zeeman effect would then provide indirect experimental evidence of spin before it was ever formally conceptualised. The anomalous Zeeman effect described the phenomenon where atoms such as hydrogen

displayed splittings into even numbered states, which was problematic as if angular momentum was quantised only as an integer, you should expect $2l + 1$ states, where $l \in \mathbb{Z}$, thus only producing odd numbered splittings. This would then later contribute to the discovery of the half-integer spin particles.

In present time, the Zeeman effect is now a well understood quantum phenomena with plenty of practical applications across various fields of physics, medicine and biology. For example, the development of the MRI machine that is used to create detailed pictures inside the human body has had countless of use cases and will continue to do so in alignment with the advancement of modern medicine. The machine relies on the knowledge brought about by the analysis of the Zeeman effect and amongst other magnetic-related theories in physics.

2 Theory

2.1 Weak Field Zeeman Effect

When an atom is placed in an uniform external magnetic field, $\mathbf{B}_{\text{ext}}$, the energy levels of the atom are shifted slightly. For a single electron, the perturbation is

$$H'_Z = -(\mu_l + \mu_s) \cdot \mathbf{B}_{\text{ext}}. \tag{1}$$

where l and s denote the orbital motion and spin of the electron, therefore

$$u_s = -\frac{e}{m}\mathbf{S}$$

which describes the magnetic dipole moment associated with electron spin and

$$u_l = \frac{e}{2m}\mathbf{L}$$

which is the magnetic dipole moment associated with the orbital motion. Therefore, Equation 1 becomes

$$H'_Z = \frac{e}{2m}(\mathbf{L} + 2\mathbf{S}) \cdot \mathbf{B}_{\text{ext}}.$$

In the weak-field Zeeman effect regime, we find that $B_{\text{ext}} \ll B_{\text{int}}$, meaning fine structure dominates and we can include the Bohr and the fine structure interactions as the unperturbed Hamiltonian and the Zeeman effect as our perturbed Hamiltonian, i.e

$$\begin{aligned} H &= H_{\text{Bohr}} + H'_{fs} + H'_Z \\ &= H_0 + H'_Z. \end{aligned}$$

The energy states in the unpertubed Hamiltonian are degenerate however if we align $\mathbf{B}_{\text{ext}}$ with the z axis, H'_Z will commute with J_Z and L^2 so the good eigenstates are

$$\langle n, l, j, m_j|$$

where each of the degenerate states can be uniquely labeled by m_j and l. Therefore, using non-degenerate perturbation theory, the first order correction to energy is

$$E_Z^{(1)} = \langle nljm_j | H_Z' | nljm_j \rangle = \frac{e}{2m} B_{\text{ext}} \langle \mathbf{L} + 2\mathbf{S} \rangle .$$

The oribtal quantum number L denotes the length or magnitude of angular momentum due to orbital motion of the electron whereas the magnetic sublevels m describes the orientation in space for L, i.e the projection onto the z-axis, therefore

$$-l \leq m \leq l$$

where $l = \frac{L}{\hbar}$. So for the lower level of the transition ${}^1P_1^o$, m' can take on the values $-1, 0, 1$ as $l = 1$.

To determine the expectation value of $\mathbf{L} + 2\mathbf{S}$, we begin with writing

$$\mathbf{L} + 2\mathbf{S} = \mathbf{J} + \mathbf{S}.$$

Since the magnetic field is aligned with the z-axis, we already know $\langle \mathbf{J} \rangle = m_j$ and we know the time average value of $\mathbf{S}$ must be its projection along $\mathbf{J}$ so

$$\langle \mathbf{S} \rangle = \frac{(\mathbf{S} \cdot \mathbf{J})}{J^2} \mathbf{J}.$$

If we square $\mathbf{L} = \mathbf{J} - \mathbf{S}$ so that $L^2 = J^2 + S^2 - 2\mathbf{J} \cdot \mathbf{S}$ and rearrange for $\mathbf{J} \cdot \mathbf{S}$

$$\begin{aligned}
\mathbf{J} \cdot \mathbf{S} &= \frac{1}{2} \left(J^2 + S^2 - L^2 \right) \\
&= \frac{\hbar^2}{2} \left(j(j+1) + s(s+1) - l(l+1) \right) . \\
&= \frac{\hbar^2}{2} \left(\frac{3}{4} + j(j+1) - l(l+1) \right) \text{ (spin of electron is 1/2)}
\end{aligned}$$

Therefore, the average value of $\mathbf{L} + 2\mathbf{S}$ is

$$\mathbf{L} + 2\mathbf{S} = \mathbf{J} + \mathbf{S} = m_j \left(\frac{3}{2} - \frac{3/4 - l(l+1)}{2j(j+1)} \right)$$

or more succintly defined using the Lande g-factor, g_j. The energy correction is then

$$\begin{aligned}
E_Z^{(1)} &= \frac{e\hbar}{2m} g_j B_{\text{ext}} m_j &(2)\\
&= \mu_B g_j B_{\text{ext}} m_j &(3)
\end{aligned}$$

where μ_B is the Bohr magneton.

We can plot Equation 2, setting $g_j = \mu_B = 1$

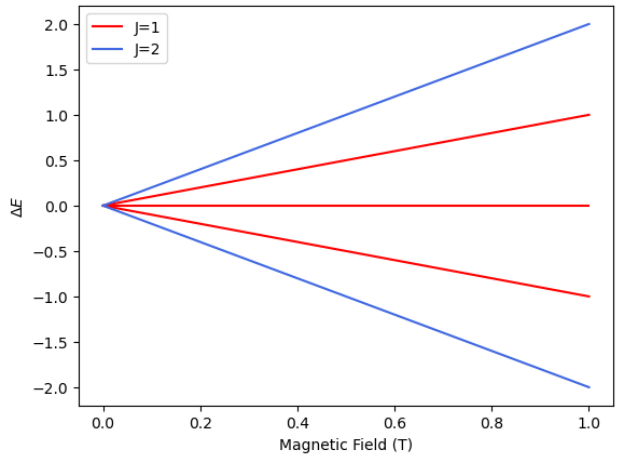

Figure 1: ΔE vs B plot showing the two different levels, $J = 1$ and $J = 2$, we find that the higher total angular momentum corresponds to a greater energy split.

We can see in Figure 1 that there are 3 sublevels for $J = 1$ and 5 sublevels for $J = 2$, however since this is an electric dipole transition and with $DeltaJ = 1$, the only allowed Δm values are $-1, 0, 1$. We can do an example calculation for an energy level splitting of ${}^1D_2$ and $1P_1^o$ in 1 T magnetic field. Using Equation 2 and with $g = 1$, we find that the splitting of the energy levels can be 0 for $\Delta m = 0$ and for $\Delta m = \pm 1$

$$\Delta E = \pm \mu_B.$$

The shift in wavelength is then

$$\Delta\lambda = \pm \frac{hc}{\Delta E} = \pm \frac{hc}{\mu_B}. \tag{4}$$

3 Experimental Setup

In this experiment, a Cd discharge lamp is placed between the poles of an electromagnet and the resultant spectral line splittings are resolved, by means of a Fabry-Perot étalon and measured, as a function of applied magnetic field, by using a CCD camera and a frame grabber to capture the images of the spectral lines. A schematic diagram of the experimental set-up is given in Figure 2

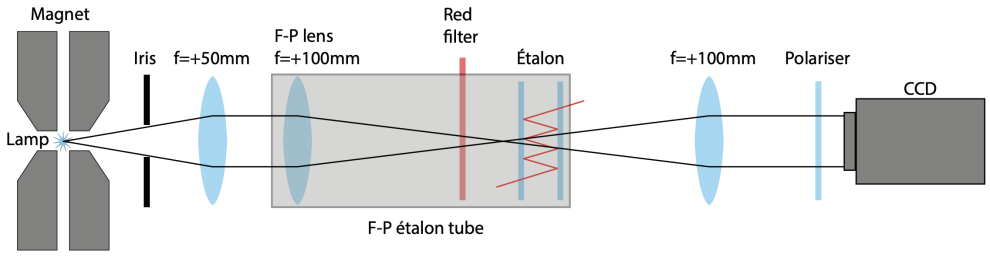

Figure 2: The beam path is idealised as it assumes the lamp is a point source. The iris and lens serves the purpose of better resolution for the CCD camera, the main instrument in this experiment is the F-P etalon.

The discharge lamp emits wavelengths 467.8 nm, 480.0 nm, 508.6 nm and 643.8 nm however with the red filter, only $\lambda = 643.8$ nm will pass through.

3.1 Fabry-Perot Etalon

The Fabry-Perot Etalon is a practical application of the more simple F-P interferometer. The F-P interferometer consists of two parallel flat glass plates, coated on the inner surface with a partially transmitting metallic layer.

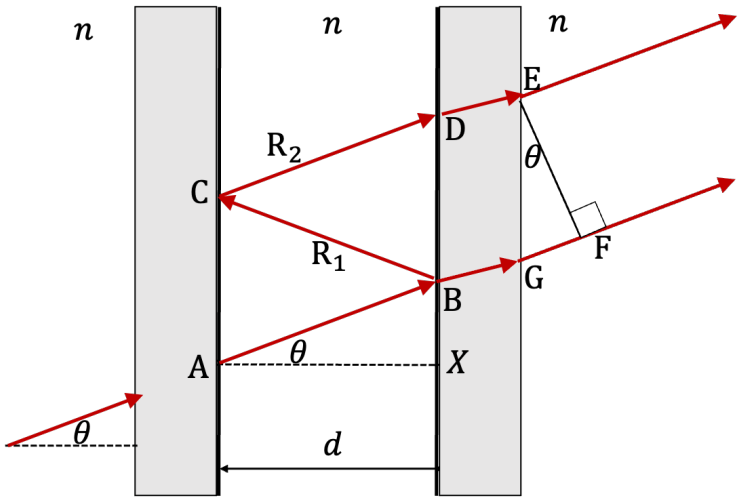

Figure 3: Diagram of the parallel plates of the Fabry-Perot interferometer. Close up to show geometry.

The two glass plates are separated by a distance d. The incoming light rays will make an angle θ at the normal as shown in Figure 3. Here we only consider 1 ray but in actuality there are infinite number of rays hitting the interferometer. We want to find the path difference between ray paths ABCDE and ABGF i.e the path from reflection and the path from the transmitted rays. The path difference is

$$\begin{aligned}\Delta OPL &= n(AB + BC + CD + DE) - n(AB + BG + GF) \\ &= n(BC + CD) - n(GF) \text{ (as DE = BG).}\end{aligned}$$

From $\triangle ABX$, we can find $AB = BC = CD$,

$$AB = \frac{d}{\cos\theta}.$$

We can find GF by considering $GF = EG\sin\theta$ where $EG = 2BX$ and $BX = d\tan\theta$ so

$$\begin{aligned}\Delta OPL &= n\left(\frac{2d}{\cos\theta} - 2d\sin\theta\tan\theta\right)\\ &= n\frac{2d}{\cos\theta}\times\cos^2\theta\\ &= 2ndcos\theta.\end{aligned}$$

Using the phase difference, we can look for constructive inteference,

$$2nd\cos\theta = m\lambda$$

where m must be an integer. As the equation depends on $\cos\theta$, we find that the higher orders tend towards the middle, therefore higher wavelengths will be towards the center, as shown in

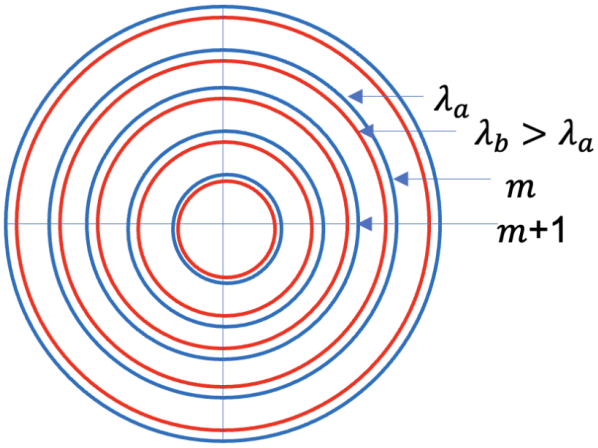

Figure 4: The higher order of interference corresponds to smaller angle as $\cos\theta_m < \cos\theta_{m+1}$ so $\theta_m > \theta_{m+1}$.

We now want to relate the radius of the rings observed on the screen with the wavelength of the incoming light. We can first take a small angle approximation.

$$\theta \approx \sin\theta = \frac{r}{f}$$

where f is the focal length of the lens on the output of the etalon, as it focuses the outgoing rays from the etalon onto the screen. We can do a first order Taylor expansion of $\cos\theta$ so

$$\cos\theta \approx 1 - \frac{1}{2}\left(\frac{r}{f}\right)^2.$$

Therefore combining with the interference condition,

$$\lambda = \frac{2nd}{m}\left(1 - \frac{1}{2}\left(\frac{r}{f}\right)^2\right). \tag{5}$$

3.2 CCD Camera

The standard sensor size for a 1.1" format is shown in Figure 5

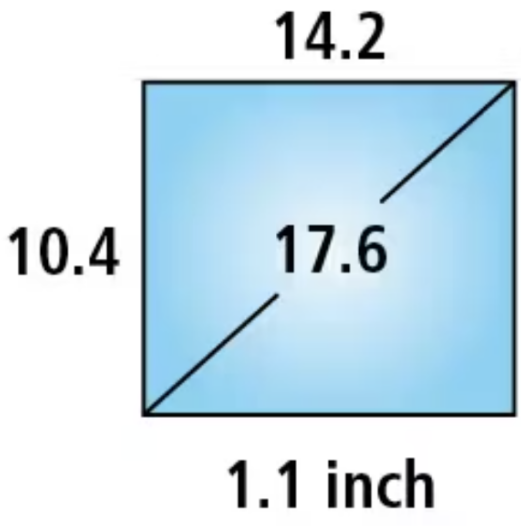

Figure 5: The dimensions of a 1.1 inch format camera, with width 14.2 mm and height 10.4 mm.

The camera's resolution is 4096 horizontal by 3000 vertical pixels so to calculate the average size of a pixel, the height is given as $10.4mm/3000$ and its width given as $14.2mm/4096$. Taking the average of the two gives us a conversion between px and mm we can use

$$\begin{aligned}\text{Pixel Length (px)} &= \frac{1}{2}\left(\frac{10.4}{3000} + \frac{14.2}{4096}\right)\\ &\approx 0.0035 \text{ mm}\\ &= 3.5\ \mu\text{m}\end{aligned}$$

However, to take the data, we magnified the image by 1.9, so the conversion between px to μm should be

$$1px = 1.84\mu m.$$

4 Results & Discussion

We opted to not complete the Field calibration exercise as it is unnecessary due to the fact that in this experiment, we are only turning up the magnetic field strength. Magnetic hysteresis only really becomes an issue if we are constantly changing the direction of the changes.

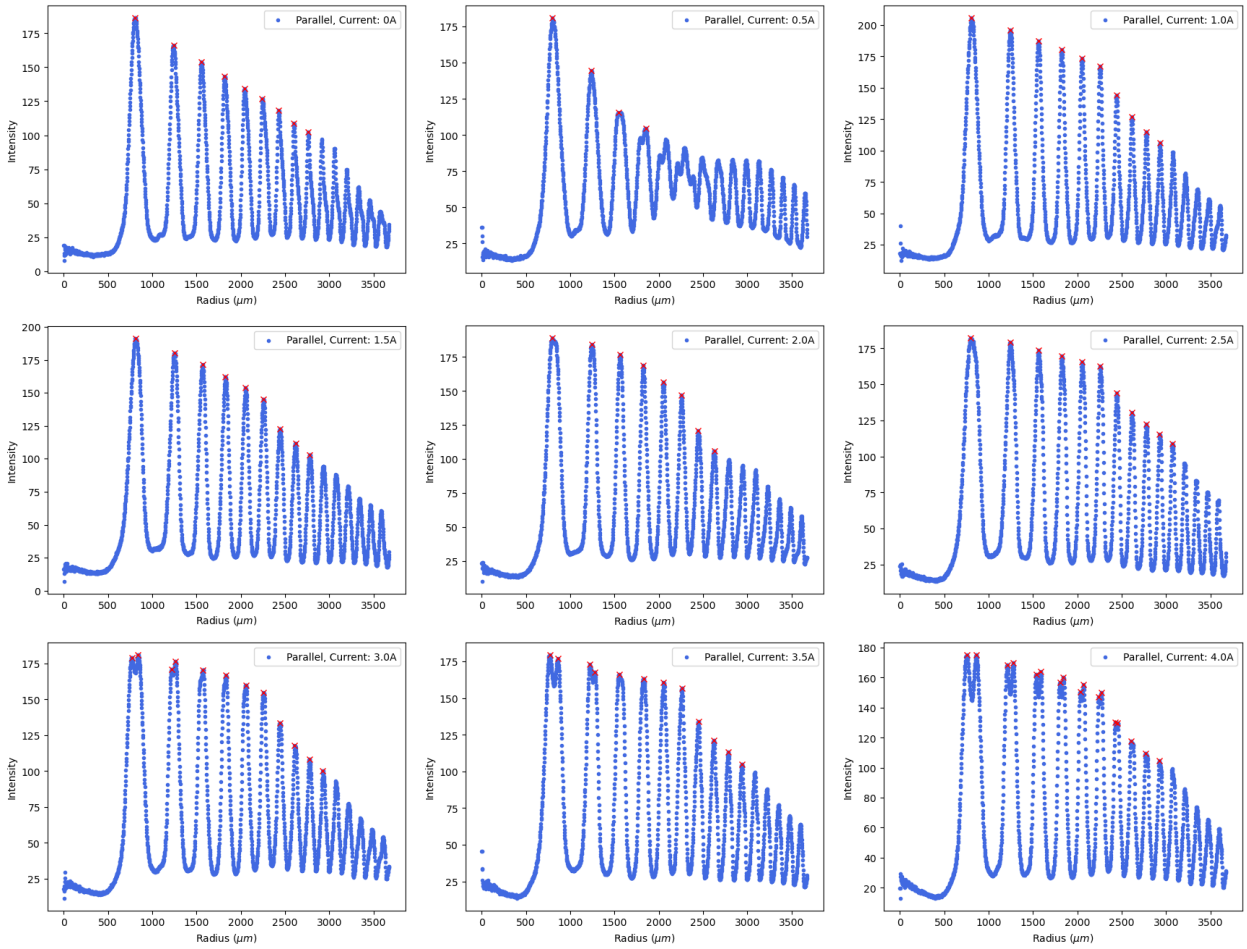

Figure 6: Intensity vs radius graphs for increasing magnetic field strengths observed parallel to the magnetic field. It is clear that Zeeman splitting only becomes apparent at 3A, or 118.9mT in this setup.

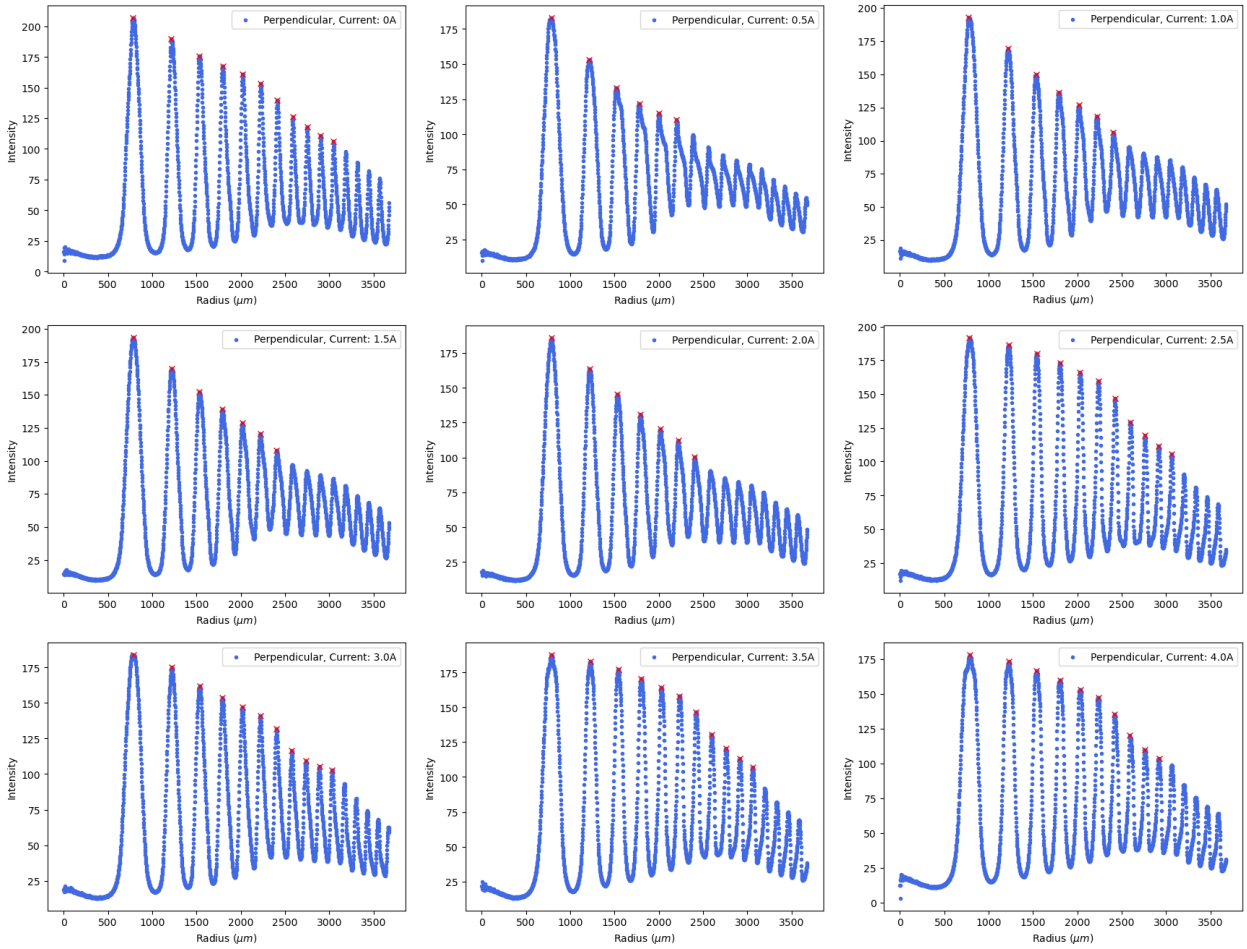

Figure 7: Intensity vs radius graphs for increasing magnetic field strengths observed perpendicular to the magnetic field. Unlike before, there is no clear Zeeman splitting in the 3A 4A range.

4.1 Bohr Magneton

To find μ_B, we looked specifically at 4A parallel observation, where there was a clear splitting into two levels.

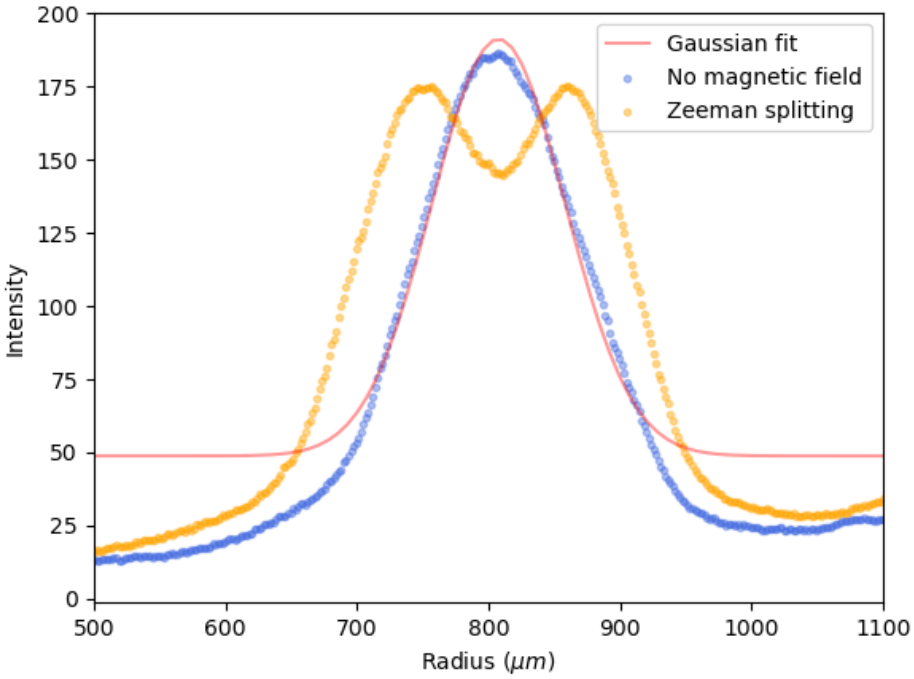

Figure 8: bluh

In Figure 8, we find peaks in the Zeeman splitting at 756.24 and 859.28 μm. This corresponds to wavelengths of 643.79 nm and 643.78 nm respectively using Equation 5. We can then convert them into energies using

$$E = \frac{hc}{\lambda}$$

where h is Planck's constant and c is the speed of light. To find ΔE we can do the following,

$$\Delta E = \frac{E_1 - E_2}{2}.$$

Finally, to obtain μ_B, we divide by the magnetic field strength $B = 143.6mT$, giving us a Bohr magneton value of

$$\mu_B = 8.95 \times 10^{-24} J/T.$$

To obtain an uncertainty value, we fit a Gaussian to the zero magnetic field observation as seen in Figure 8. We obtain a full width at half maximum reading of 119.11, leading to a standard deviation of 50.6. Therefore, the two radii readings used in the calculation has a percentage uncertainty of 6.7% and 5.9%. Adding them in quadrature gets us a total random uncertainty of 8.9%. Thus, our experimental value for the Bohr magneton is

$$\mu_B = 8.95 \pm 0.8 \times 10^{-24} J/T.$$

This result agrees with the widely accepted value of $\mu_B = 9.27 \times 10^{-24} J/T$.

4.2 Polarisation

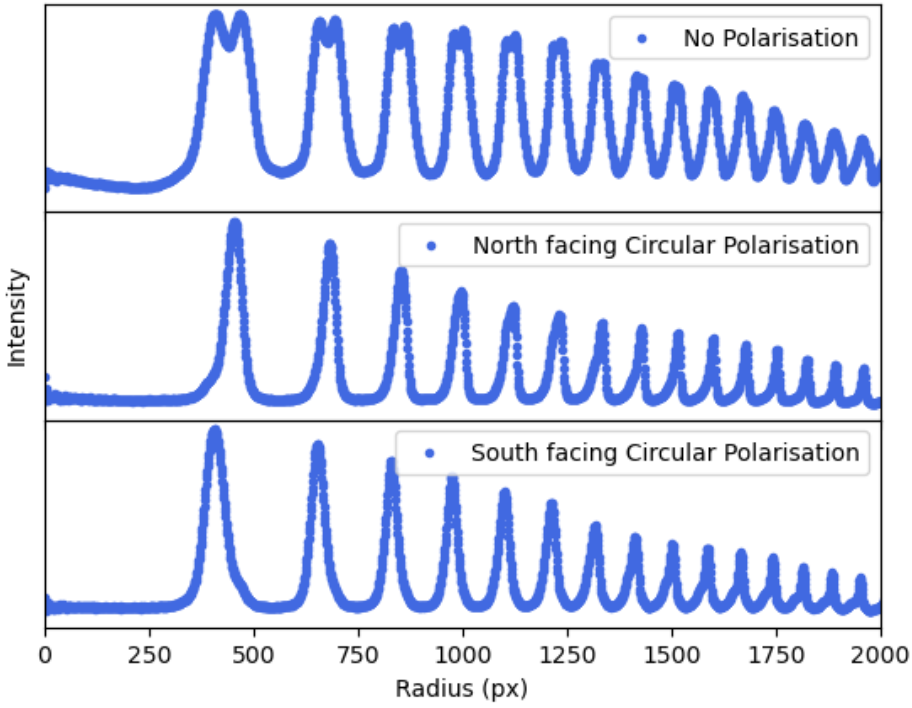

Figure 9: Intensity graphs comparing the three setups viewing parallel to the field: no polariser, right-handed polariser and left-handed polariser.

In Figure 9, we can see that the Zeeman splitting has two levels that are differed in their polarisation. Therefore, the $\Delta m = \pm 1$ are circularly polarised, i.e σ^+ component is right-handedly circular polarised and σ^- is left-handedly circuarly polarised.

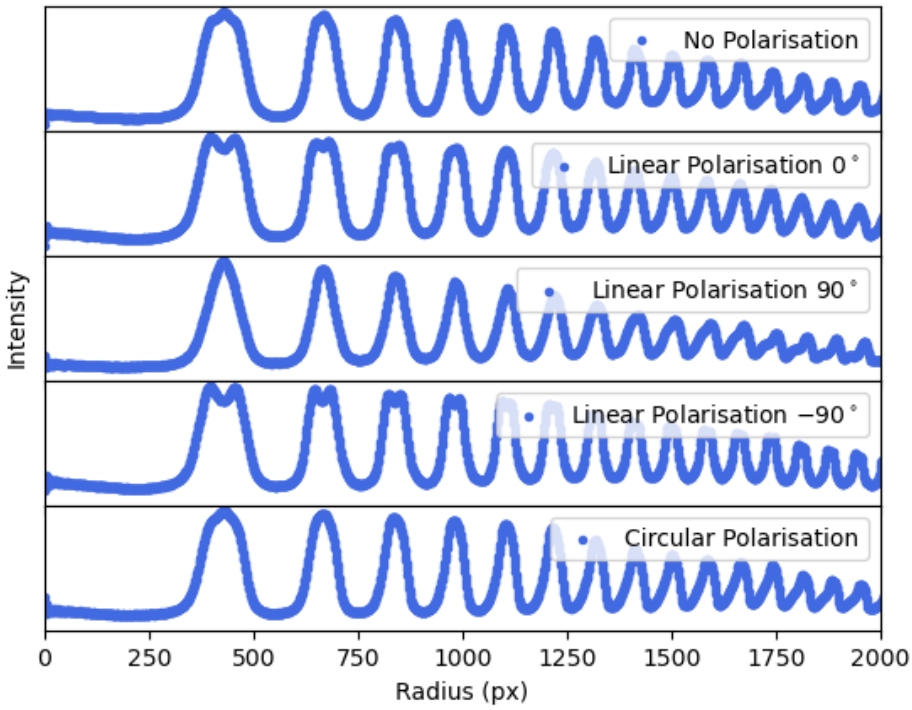

Figure 10: Intensity graphs comparing 5 setups viewing perpendicular to the magnetic field: no polarisation, linear polariser at 0°, 90°, −90° and circular polariser.

In Figure 10, we can see that the lack of Zeeman splitting is not because there is no Zeeman splitting. It is because our equipment is not sharp enough to resolve the different levels. From the polarisation experiment, we can see that there is a linearly polarised level, $\Delta m = 0$, or commonly expressed as π component. We can also see in the circular polarisation that it had no effect however we think that this is a low resolution result rather than expected polarisation.

5 Conclusion

In conclusion, we successfully determined the different polarisation of the Zeeman splitting levels whilst also finding a value for the Bohr magneton. In future, we want to take more accurate measurements as the sensitivity levels in each variable to the result was quite high.